Tailoring the surface morphology of polyimide for improved adhesion

by R. F. Saraf J. M. Roldan T. Derderian

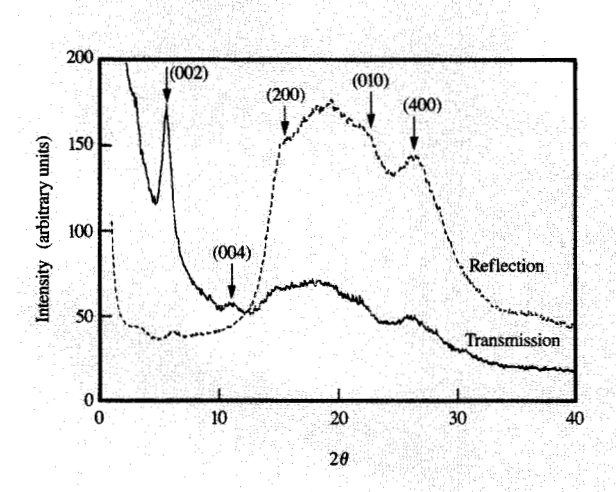
Semiflexible polyimide structures are not amenable to good adhesion because of their a) spontaneous orientation of the polymer chains parallel to the film substrate during curing, b) formation of an ordered skin, and c) smooth surface topography. We briefly discuss these structural features with regard to metal-onpolyimide (metal/PI) adhesion. A method is proposed to improve adhesion by tailoring the surface and bulk morphology of the PI to circumvent these properties. In this method, different precursors of the same polyimide (PMDA-ODA) are blended. Phase separation induces spontaneous roughening of the PI surface. This novel technique reduces the extent of chain orientation, gives rise to topographical and morphological surface heterogeneities, and produces a discontinuous ordered skin. A variety of topographical features with nanoscale dimensions are produced that range from "mounds" to "dimples." The process does not alter the overall chemical composition of the PI, occurs spontaneously, and is extendable to other

polyimides or polymer systems. Threefold and ninefold enhancements of adhesion over that of a conventionally cured PMDA-ODA film are obtainable for electroless and vapor-deposited Cu on PI, respectively.

1. Introduction

Semiflexible and mesomorphic polyimides are used in the microelectronics industry for applications in chip packaging [1] and as high-performance composites in the aerospace industry because of their low dielectric constant, good mechanical properties, stability at high temperatures, and low thermal expansion coefficients. Although hightemperature polyimides such as poly(pyromellitic dianhydride-oxydianiline) (PMDA-ODA) and poly(biphenyl dianhydride-p-phenylene diamine) (BPDA-PDA) are insoluble (except in concentrated sulfuric acid [2]), they can be processed in their precursor acid or ester forms [3]. The solubility of the precursor in polar solvents such as N-methyl pyrrolidinone (NMP) leads to processibility, increasing the utility of this class of rigid, high-temperature polymers. In recent years, UVlight-sensitive polyimides, referred to as photosensitive

^eCopyright 1994 by International Business Machines Corporation. Copying in printed form for private use is permitted without payment of royalty provided that (1) each reproduction is done without alteration and (2) the Journal reference and IBM copyright notice are included on the first page. The title and abstract, but no other portions, of this paper may be copied or distributed royalty free without further permission by computer-based and other information-service systems. Permission to republish any other portion of this paper must be obtained from the Editor.



BE STORY

WAXS spectra of a PMDA-ODA film imidized from PAA. The sample was soft-baked at 70°C for 30 min, followed by a 10°C/min ramp to 410°C. The hard bake at 410°C was carried out for 60 min in a forming gas atmosphere. The film was 127 μ m thick. The diffractograms are corrected for absorption, and the spectrum in transmission is multiplied by 3.

polyimides, have been synthesized for potential use as imageable dielectric materials for high-performance multilayer structures in chip packaging [4, 5]. The importance of polyimides is further augmented by their application as a matrix material in constructing high-performance composites in the aerospace industry [6]. PI copolymers have also been constructed for use as structural adhesives in both the aerospace and microelectronics industries [7].

In one of their salient applications, PI films $\sim 1-50~\mu m$ thick are used as a dielectric layer in multilayer structures for chip packaging. This application requires good metal/PI adhesion for circuitry. For copper films in circuits, adhesion to PI is established by first depositing a thin adhesion layer of chromium (10–50 nm) [8]. The chromium (Cr) forms complexes with the PI aromatic ring, enhancing adhesion [9]. However, the Cu/Cr/PI structure can absorb moisture at the Cr/PI interface which oxidizes the Cr and causes a brittle failure [10]. The need for "adhesiveless copper laminates" becomes more pronounced with the increased performance requirements of processors and packages, including circuitry on flexible substrates (referred to as flex circuits).

Metal adhesion to a cured PI surface is typically poor. In this paper, we suggest that the poor metal adhesion to a PI surface arises as a result of the intrinsic (physical) structure of the polymer film and its surface. The features of a semiflexible PI film that could contribute to poor

adhesion are 1) Smoothness of the PI film surface at nanoscale levels. The typical root-mean-square (rms) roughness of a PI film is <1 nm for a lateral sampling dimension of $\sim 10^2$ nm. 2) The spontaneous alignment of PI chains parallel to the film plane during imidization, which leads to a planar texture (discussed below). The planar texture forms a "mica-like" structure that tends to delaminate in the film plane. 3) A more ordered near-surface region (top 10 nm), or "skin," of semiflexible PI with a higher percent crystallinity and degree of chain orientation (relative to the bulk) that is aligned parallel to the film plane. These differences between the skin and bulk morphologies increase the tendency for the skin to delaminate from the bulk, leading to a weak skin/bulk interface. We refer to this phenomenon as the skin effect.

Simply modifying the surface topography [11–13] is not sufficient to improve adhesion, since polymer morphology (features 2 and 3, above) also plays an important role. These morphological attributes were previously reported, as mentioned below, but their relation to poor adhesion was not appreciated. We have developed a procedure [14] that alters the structure of the PI such that the planar orientation is diminished, the skin is not continuous, and the surface roughness increases significantly at a nanoscale level with good planarity on a micron scale. Each of these changes occurs spontaneously during imidization and does not require additional processing steps. Only semiflexible polyimide films, referred to as polyimides (PI), derived from PMDA-ODA are discussed in this paper, although the structural attributes of poor adhesion and the means proposed for their modification should apply equally to other polyimides and polymer systems.

This paper is divided into three parts: In Section 2, the PI structural features and their relation to poor adhesion are discussed; in Section 3, the procedure that alters the PI structural features is presented; and in Section 4, the adhesion strengths of Cu deposited on a film prepared by conventional curing methods and by this new procedure are compared.

2. Effect of polyimide morphology and topography on adhesion

In this section, the structural features of PMDA-ODA film that affect its adhesion properties are briefly described. First, the planar texture of the film is studied using wide-angle X-ray scattering (WAXS). The tendency of films with a planar orientation to delaminate is illustrated in a scanning electron microscope (SEM) micrograph. In the next subsection, the skin effect is demonstrated, using a grazing incidence X-ray scattering (GIXS) method. The weakness in the skin/bulk interface is explained by considering the overall shape of the oriented polymer chains. The smoothness of the PI surface is measured using X-ray reflectivity in the subsection which follows.

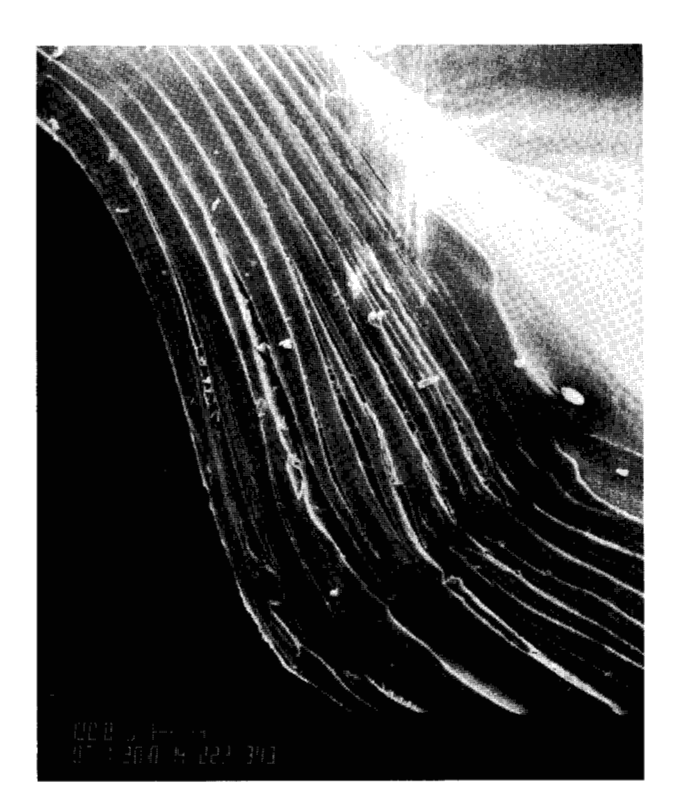
Synchrotron X-ray techniques are used to perform the measurement at a resolution depth (i.e., root-mean-square roughness) of less than 0.1 nm, with a lateral sampling length greater than 100 nm.

• Planar orientation

A wide-angle X-ray scattering (WAXS) pattern of PMDA-ODA soft-baked at 70°C to remove solvent and then cured (hard-baked) to 410°C at 10°C/min is shown in **Figure 1**. The indexing of the WAXS pattern reported for PMDA-ODA indicates either an orthorhombic [15, 16] or monoclinic [17] structure with one chain per unit cell. However, a crystal structure calculation which allows for perturbations in the chain conformation and interchain differences indicates that two chains per lattice cell is more suitable [18], and our indexing is based on the latter structure. The PI structure corresponds to a 2/1 helix chain with a pitch of 3.29 nm (= c), forming orthorhombic packing with a = 1.32 nm and b = 0.39 nm [18].

The intensity of the (002) peak corresponds to the periodicity along the chain at scattering angle $2\theta \sim 5.6^{\circ}$. Relative to other peaks, it is significantly higher in the transmission than in the reflection mode. Since the momentum vector is parallel and perpendicular to the film surface for transmission and reflection modes, respectively, a relative increase in the (002) intensity indicates that PI chains are oriented parallel to the film surface or substrate (X-Y) plane. Since the chain does not have any preference between the X- and Y-axes in the film plane, the chain (i.e., c-axis) is randomly oriented in the X-Y plane. This orientation has previously been reported by measuring refractive indices in three directions, along X-, Y- and Z-axes [19]. WAXS plots can probe the chain orientations along the a- and b-axes. When the peaks are indexed on the basis of a calculated structure [18], the (010) and (400) peaks are present in diffractograms measured in reflection and transmission mode. The relative peak heights are nominally invariant, indicating that the aand b-axes are randomly oriented around the c-axis. Such an orientation distribution is defined as planar texture [20]. Chain orientation parallel to the X-Y plane has been observed [19], but the planar texture was not inferred from the observations. The extent of orientation of the c-axis with respect to the Z-axis (perpendicular to the film plane) is discussed below. A spontaneous planar orientation of a chain axis during imidization is a special characteristic of PI films. Planar texture in flexible, semicrystalline polymers, such as isotactic polypropylene (i-PP) and poly(ethylene terephthalate) (PET), must be induced by equibiaxial deformation [21].

Next we discuss the effect of planar texture on adhesion. In uniaxially deformed semicrystalline polymers, the mechanical strength and tensile modulus in the draw

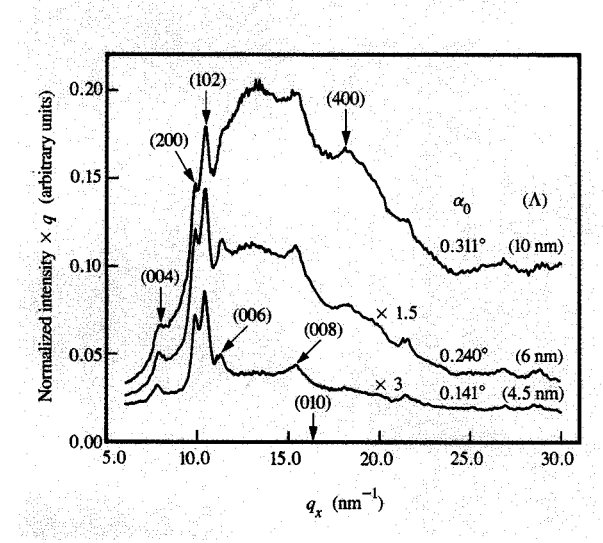


2101117:30

SEM micrograph of a freeze-fractured edge of a uniaxially compressed isotactic polypropylene (i-PP) sample at 140°C at a compression ratio of 25× [22]. The sheet-like delamination parallel to the film surface is attributed to the planar orientation of the polymer.

(i.e., deformation) direction increase with a concomitant decrease in the transverse direction [22]. Analogous to fiber orientation, for chain orientation parallel to the film plane, the strength in the planar direction improves, but the strength and modulus in the thickness (Z) direction decrease. Highly oriented, high-strength fibers fibrillate on bending because of easy crack propagation in the fiber direction [23]. Similarly, planar-oriented polymer films can easily delaminate in the film plane. Figure 2 shows an equibiaxially deformed fractured film of i-PP which has a planar-oriented chain axis. The equibiaxial deformation that induces planar chain orientation was achieved by a uniaxial compression [24]. The fracture occurred after the film was immersed in liquid N, followed by a single stroke with a pair of tweezers at the film's edge. As in biaxially deformed i-PP, the spontaneous planar orientation of PI chains enhances film delamination parallel to the X-Y plane irrespective of the (specific) chemical interaction at the interface. Consequently, an interface with a planar-

Y. C. Cohen and R. F. Saraf, unpublished result, 1986.



Falle

GIXS spectra of a PMDA–ODA polyimide film on silicon formed by CVD technique under high vacuum. The incident and scattering grazing angles α_0 and α_0' are equal and constant for a given scattering curve. The sampling depth Λ increases with the grazing angles α_0 and α_0' . The grazing angles for the three curves with sampling depths of 4.5 nm, 6.0 nm, and 10.0 nm are 0.141°, 0.240°, and 0.311°, respectively. The 0.6-nm rms roughness and critical angle for total reflection $\alpha_c = 0.171^\circ$ are determined by performing X-ray reflectivity measurements on samples prepared under identical conditions.

oriented PI film decreases the adhesion strength between metal and PI.

• Near-surface ordering: Skin effect

Another aspect of PI morphology that leads to poor adhesion is the skin effect observed in conventionally processed PMDA-ODA films. The near-surface structure of a PI film can be probed by a GIXS technique. In this method, an X-ray beam is incident below the critical angle (~0.18° with respect to the surface for PMDA-ODA for the X-ray wavelength, $\lambda = 0.156$ nm). Scattering from the evanescent wave produced by the total reflection condition is usually measured at this same grazing angle. Since both the incident and scattered beams are nominally parallel to the surface, the in-plane structure of the PI film can be determined. By increasing the grazing angle, structures 10⁰ to 10³ nm deep from the surface are measured with a 1-10-nm depth resolution [25]. GIXS spectra from PMDA-ODA films cured to 410°C show a significant enhancement in (local) ordering within ~10 nm of the air/polymer interface [26].

An analysis of GIXS spectra at larger scattering angles corresponding to momentum vector q > 5.0 nm⁻¹ for

CVD-grown film (see **Figure 3**) shows some distinct features²: 1) surface ordering is similar to that of conventionally cured PI film; 2) the (010) reflection at $q \sim 16.0 \, \mathrm{nm^{-1}}$ present in the bulk sample (see Figure 1) is absent; and 3) the (200) reflection is strong and decreases at greater depths relative to the (102) reflection. CVD films are made solvent-free by depositing the two monomers simultaneously on the substrate followed by curing.

Observation 1 indicates that the formation of a highly ordered skin is probably a consequence of PI surface mobility. GIXS measures the structure parallel to the film surface. From observations 2 and 3, the absence of (010) and the presence of (200) and (102) reflections indicate that the polymer chains in the ordered phase are oriented such that the unit cell a-axis is parallel and its b-axis is normal to the surface. Thus, the skin layer has a fiber-like texture in which the b-axis is normal to the Z-axis, and the aand c-axes are randomly oriented around the b-axis and parallel to the X-Y plane. The fiber axis is along the baxis, and is referred to as b-axis fiber texture. From the calculated crystal structure, a b-axis orientation normal to the surface implies that the benzene rings in PI tend to align parallel to the surface. Thus, the morphology in the near-surface skin layer differs from that of the bulk with respect to both higher-order and crystalline texture. As mentioned earlier, such a difference between the bulk and the near-surface region is referred to as the skin effect.

Next we consider the effect of ordered, planar-oriented skin formation on the interfacial properties. The average overall shape of the polymer chain due to planar orientation is an oblate ellipsoid (with its major axis parallel, and a minor axis normal, to the film surface), as observed by small-angle neutron scattering for a planaroriented i-PP [27]. On the average, the chain segments of the polymer molecule tend to lie in one plane parallel to the surface. As a consequence, the adjacent planes are intertwined with fewer chain segments than in an isotropic sample. In PMDA-ODA the chains in the skin are more ordered and more planar-oriented, and have larger chain extension compared to the bulk. Fewer chain segments intertwine between the skin and the bulk than between adjacent layers in the bulk. Therefore, a weak skin/bulk interface is expected to produce an interface with inferior toughness. This weakness can result in adhesion failure by delamination at the skin/bulk interface. The existence of a weak boundary layer is accounted for by the skin effect [28]. In XPS studies, chemical surface analyses of freshly peeled metal strips reveal that the locus of failure occurs in the PI even for interfaces with inferior metal/PI adhesion. Such a weak skin/bulk interface leading to poor interfacial

² R. F. Saraf, C. Dimitrakopoulos, S. P. Kowalczyk, and M. F. Toney, unpublished results.

toughness is also observed in liquid-crystalline polymers [29].

• Surface roughness

The last structural feature of PI causing poor adhesion is smooth PI surface topography. The rms roughness of a film can be measured by an X-ray reflectivity technique [30]. By using synchrotron radiation that has a spatial coherence greater than 500 nm, the rms roughness is averaged over a large area [30]. The rms roughness for PMDA-ODA is measured to be less than 1 nm for a typical film cured to 400°C using a standard thermal cycle [31]. Surface roughness in the 10^{-1} to 10^{0} - μ m range is reported to enhance (mechanical) adhesion between polymers, such as i-PP, acrylonitrile-butadiene-styrene, high-density polyethylene (HDPE), and metals such as nickel, copper, and aluminum [11-13, 32-34]. Improved adhesion on a roughened surface is due to mechanical interlocking and an increased surface area at the interface. A metal can be electrolessly plated onto a rough polymer surface using palladium as a seed [12, 13], or the polymer may be deposited by melt (or solution) processing onto a roughened metal surface [11, 33]. The roughness in semicrystalline polymers such as i-PP, HDPE, and nylon is achieved by relying on a differential rate of etching of crystalline and amorphous regions [12, 13, 34]. Polymer/metal adhesion improves as the size of the surface features decreases from a 1-\mu to a 0.1-\mu scale [35]. For PMDA-ODA films, a 10- to 100-fold increase in rms roughness averaged over a large area should improve adhesion properties.

3. Adhesion enhancement

To improve adhesion to PI surfaces, a novel method is proposed that alters the structural features of PI, i.e., a planar orientation, a smooth topography, and an ordered skin. In this section, a description of the method is followed by a brief discussion of the resultant PI structure as inferred from X-ray scattering and atomic force microscope (AFM) studies. There are three structural changes due to this processing scheme that most significantly affect the adhesion properties of the film. First, the film topography is substantially roughened at a nanoscale level. The roughening is not deliberate, but occurs spontaneously during the drying and imidization cycle. Second, the surface and the bulk are heterogeneously ordered with discretely ordered or disordered domains whose lateral dimensions range between ~ 0.1 and 10 μ m depending on the processing conditions. Such a heterogeneous morphology disrupts the uniformly ordered film that can cause skin/bulk delamination. Finally, a decrease in the planar orientation of the PI chains in the film reduces the delamination tendencies.

Acid (PAA) and ester (PAETE) precursors of PMDA-ODA are blended in a common solvent (NMP) to produce a single-phase ternary solution which is spun onto a suitable substrate. Glass disks 3/16 in. thick are used as substrates for adhesion measurements, and single-crystal Si wafers are substrates for atomic force microscope (AFM) studies. The deposited film is soft-baked at 70°C on a hot plate flushed with N₂. As the solvent evaporates, the film begins to separate into PAA-rich and PAETErich phases. The solvent NMP forms complexes with both PAA [36] and para-PAETE, but not with meta-PAETE [37]. Since the PAETE chain in this study contains both para- and meta-isomers, the PAA chain forms complexes with more NMP molecules than the PAETE chain. As a result, the PAA-rich phase swells more than the PAETErich phase. Figure 4 shows an AFM surface topograph of a blend of 20% PAA and 80% PAETE (by weight) after a soft bake. [A blend of x\% PAA and y\% = (100 - x)PAETE is referred to as x/y.] The minority component (PAA) forms the discontinuous PAA-rich phase (DPAARP) that is elevated with respect to the continuous PAETE-rich matrix (CPATRP) with excess NMP [38]. The uniform size distribution of the DPAARP "mounds" is due to phase separation by spinodal decomposition. In a 60/40 blend after soft bake, the continuous PAA-rich phase (CPAARP) forms the matrix around the discrete PAETErich phase (DPATRP). Since the CPAARP is more swollen than the DPATRP, the latter forms discrete "dimples" on the surface. The resulting topography for a 60/40 blend after a soft bake is shown in Figure 5.

The next step is to imidize the phase-separated domains by a hard-bake cycle at 400° C in a N_2 atmosphere. Both PAA and PAETE imidize to a chemically identical PI after the hard-bake cycle. The next three subsections describe changes in the physical structure due to the hard-bake process, the resultant morphology derived from WAXS and AFM analyses, and the mechanism that produces the modified PI structure. An understanding of this mechanism is necessary in order to appreciate the process and its potential for extendibility to other polymer systems.

• Surface topography

In this section, the spontaneous nanoscale roughening is described, and the mechanism of the observed topography is discussed. Based on threshold temperatures and the activation energy for imidization, the rate of imidization is \sim 15 times faster for PAA than PAETE [39]. PAA imidizes first to PI(1), followed by PAETE imidization to PI(2). Only \sim 5% PI(2) is formed when \sim 80% imidization to PI(1) is complete. Consider the PAETE-rich blend (i.e., 20/80) first. As PAA \rightarrow PI(1), the DPAARP converts to a rigid insoluble PI(1) phase, whereas the PAETE-rich matrix remains relatively unconverted and soft. As the PAETE matrix imidizes to PI(2), forming a continuous PI(2) phase,

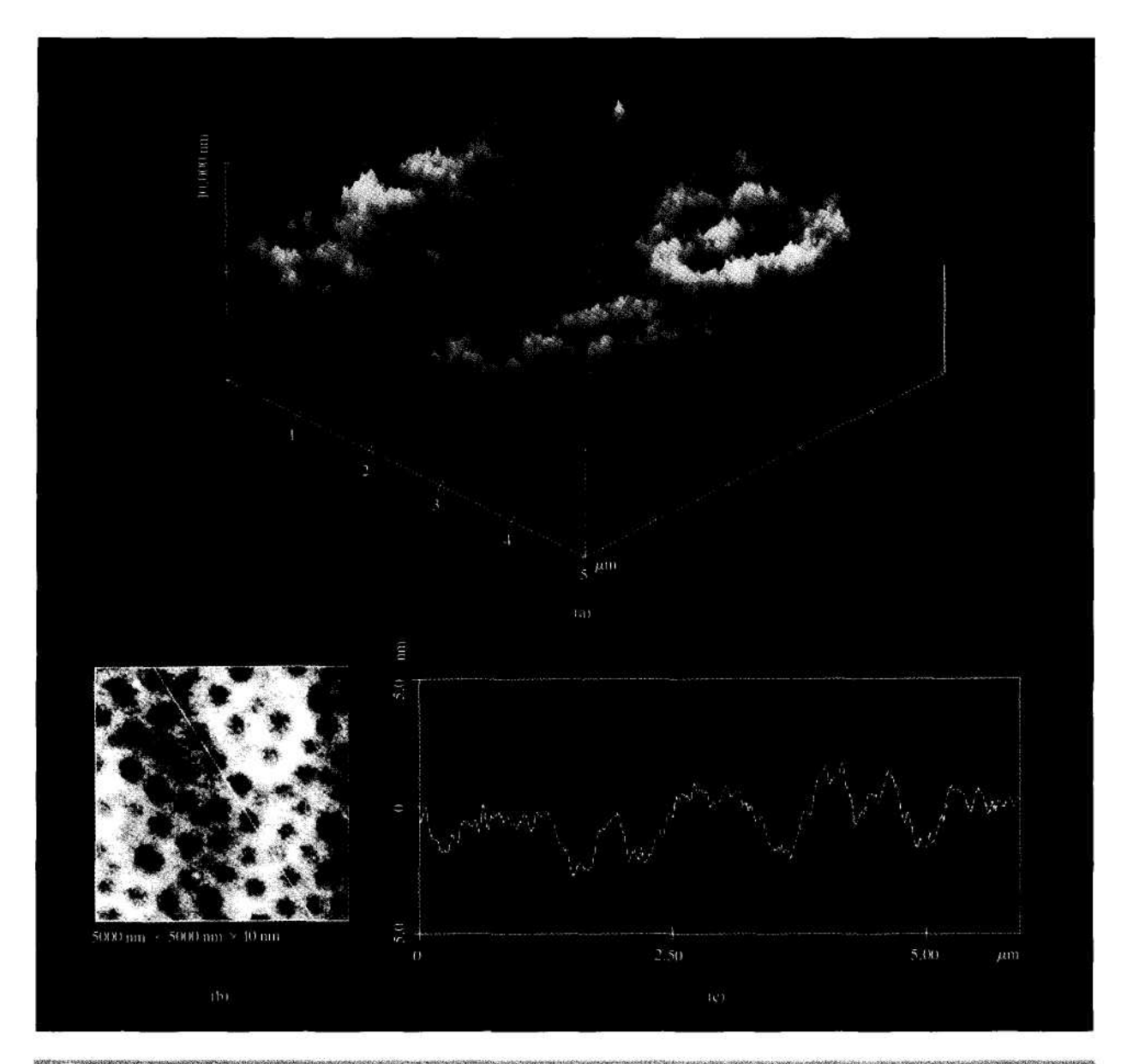
445

(a) 5×5 - μ m AFM micrograph of 20/80 blend soft-baked at 70°C. The film was made from 94% NMP solution. The thickness of the film after soft bake was 206 nm. The mounds are PAA-rich regions swollen due to the presence of complexed NMP. The large mounds are \sim 12 nm high, with a 0.58- μ m diameter at the base. (b) Top view and locus of cross section. (c) Corresponding cross-sectional view of the surface along the indicated locus.

it pushes against and elevates the PI(1) phase due to PI(2) shrinkage. The final morphology after hard bake is mounds of PI(1) surrounded by the PI(2) phase. Note that chemically the PI(1) and PI(2) phases are identical, but the extent of order in each phase may differ. Figure 6 shows an AFM micrograph of a 20/80 blend after hard bake. The comparison of the cross-sectional views in Figures 4(c) and 6(c) show that the lateral dimensions of the PAA-rich and

PI(1) phase mounds are nominally equal, indicating that the difference in rates of imidization between PAA \rightarrow PI(1) and PAETE \rightarrow PI(2) is large enough to fully maintain the phase-separated morphology.

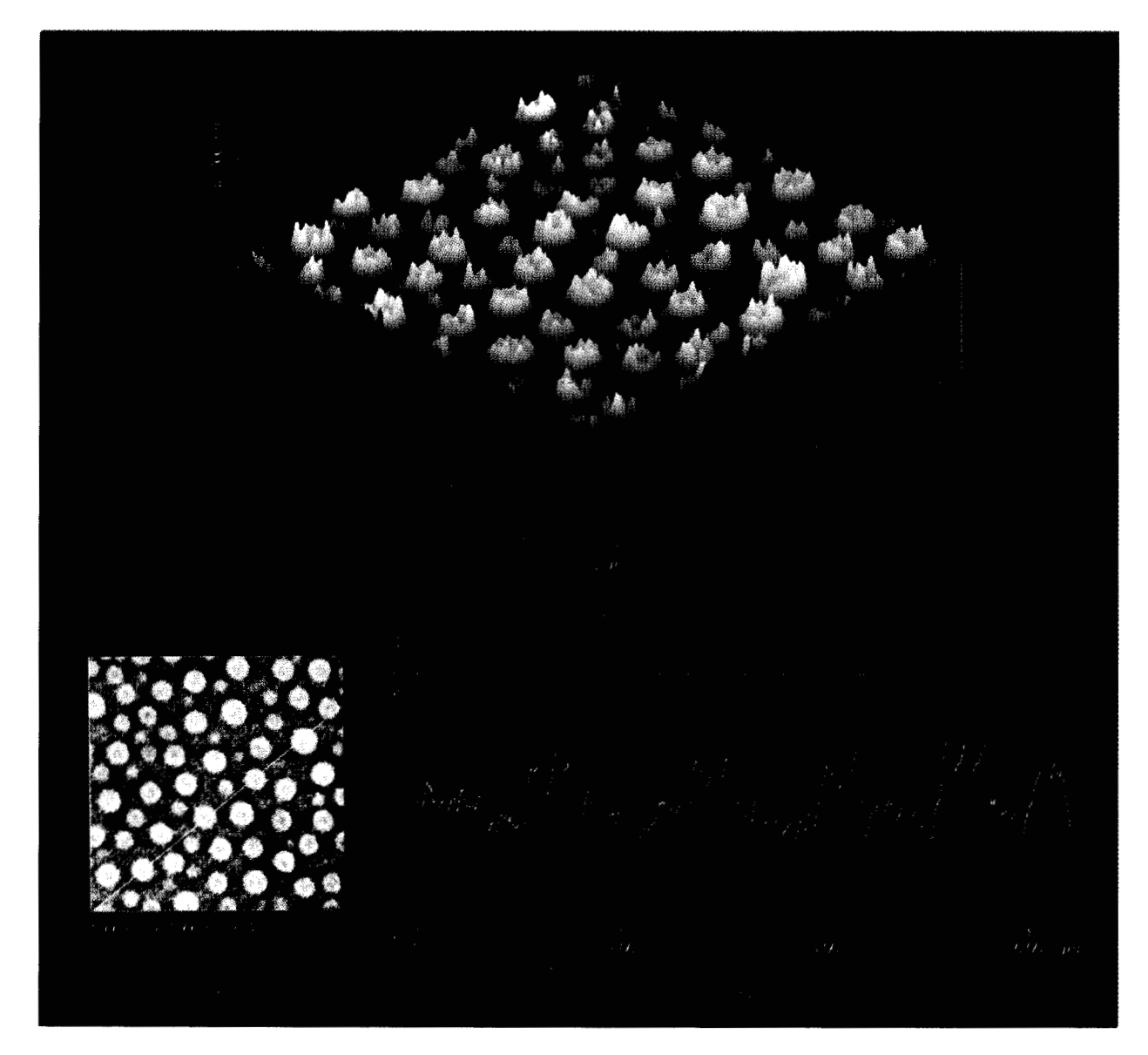
In blends with a PAA-rich composition, the topography reverses, as indicated in the micrograph shown in Figure 5. First, the CPAARP imidizes to form a continuous PI(1) phase, while the DPATRP "dimples" are not imidized.



(a) 5×5 - μm AFM micrograph of 60/40 blend soft-baked at 70°C. The film was made from 94% NMP solution. The thickness of the film after soft bake was 126 nm. The dimples are due to the swollen PAA-rich "land" relative to the phase-separated, discrete PAETE-rich regions. The large dimples are \sim 2 nm deep, with a diameter of 0.45 μm . (b) Top view and locus of cross section. (c) Corresponding cross-sectional view of the surface along the indicated locus.

Then the DPATRP imidizes to PI(2) to form a discontinuous PI(2) phase. We note that initially, as PAA \rightarrow PI(1), the depth of the dimples is reduced because of CPAARP shrinkage, but the elevation difference is enhanced during the second process of PAETE \rightarrow PI(2). Figure 7 shows the topography of the 60/40 blend after hard bake. When the cross-sectional views in Figures 5(c) and 7(c) are compared, the lateral size of the dimples is

changed insignificantly by a hard bake, indicating that phase-separation morphology is fully maintained as PAA and PAETE imidize in a manner similar to the PAETE-rich case. Although the lateral dimensions of the dimples are equal in Figures 5 and 7, the elevation difference in Figure 7 increases significantly during hard-bake curing, as seen in the cross-sectional view [Figures 5(c) and 7(c)]. The corresponding change in elevation in Figures 4(c)



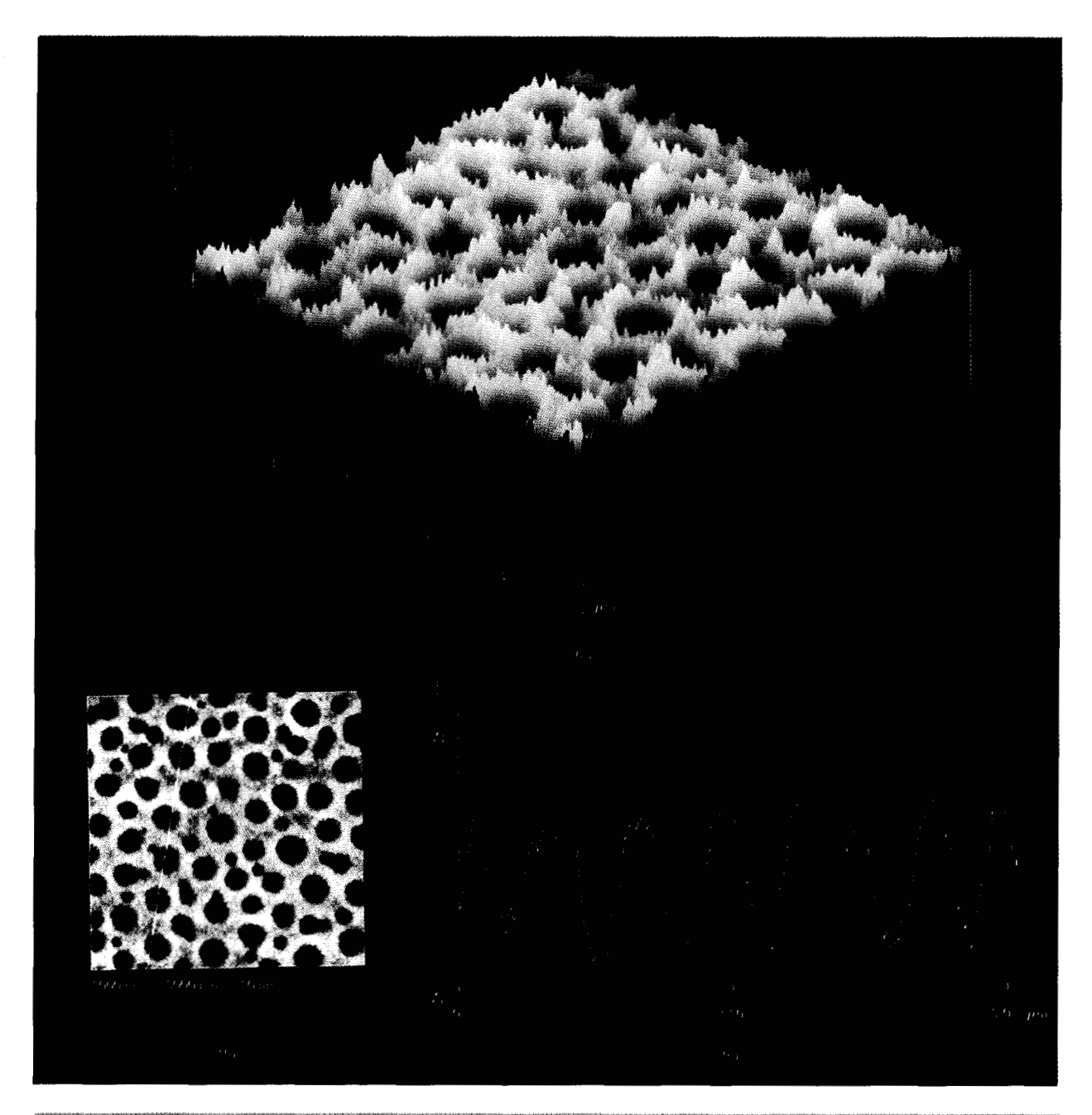
To the same of the

(a) AFM micrograph of a sample identical to the one in Figure 4 after hard bake at 400° C in a forming gas atmosphere. The diameter of the mounds is invariant, but the height shrinks to \sim 4 nm. (b) Top view and locus of cross section. (c) Corresponding cross-sectional view of the surface along the indicated locus.

and 6(c) is not as significant on curing for PAETE-rich blends [38].

We next consider a third topography, shown in Figure 8. The topography consists of three features: a) large mounds of wide size distribution; b) small, uniform-size bubbles on the large mounds; and c) small, uniform-size bubbles on the areas surrounding the large mounds. This structure is formed by casting a film from a two-phase solution of PAA/PAETE/NMP followed by a hard bake. Because of

the low surface energy of PAETE relative to PAA, the PAA-rich phase forms a discrete phase, PAARP, in the continuous matrix of the PAETE-rich phase, PATRP. On imidization, PAARP forms discrete PI(1) domains surrounded by a continuous PI(2) domain. As in Figure 4, the discrete PI(1) domains are elevated and form PI(1) mounds, as seen in Figure 8(a) with respect to the surrounding, continuous PI(2) region. The diameters of these large PI(1) mounds range from 13 to 40 μ m because



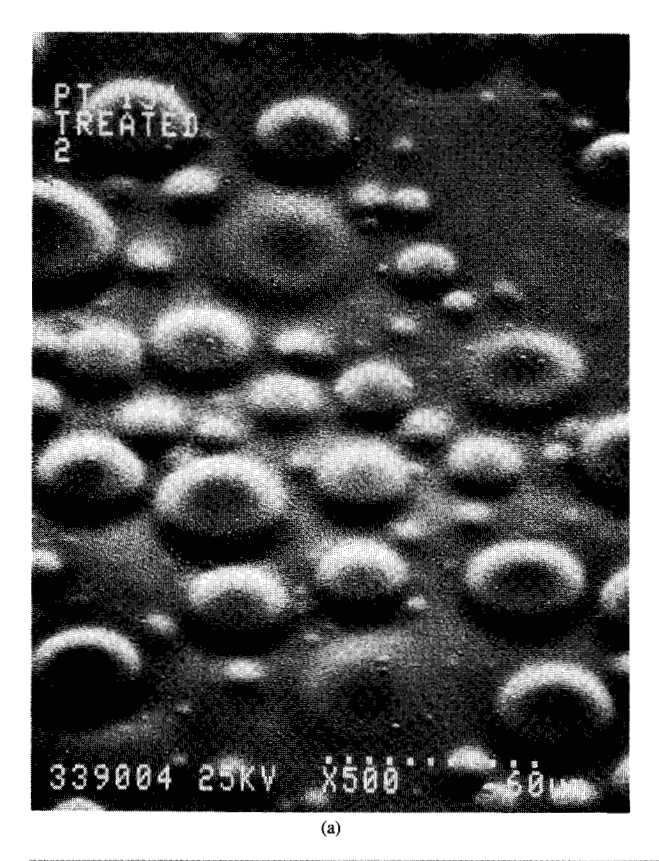
(a) AFM micrograph of a sample identical to the one in Figure 5 after hard bake at 400° C in a forming gas atmosphere. The diameter of the dimples is invariant, but the depth increases to ~ 23.5 nm. (b) Top view and locus of cross section. (c) Corresponding cross-sectional view of the surface along the indicated locus.

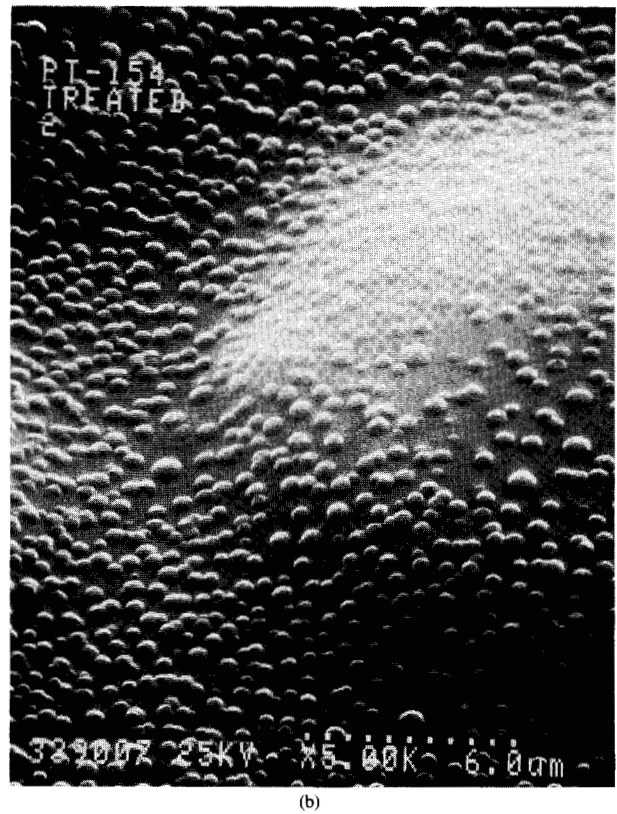
of the inhomogeneities present during the mixing process. The small depression in the middle of the mound is caused by the release of complexed NMP solvent during the hard bake (as in Figure 6).

The bubbles on the mounds form as follows: As PAA in PAARP imidizes to PI(1) during hard bake, the shrinkage

squeezes out the PAETE to form bubbles on the PI(1) mounds. The sites of extrusion of these PAETE bubbles on the surface of PI(1) mounds are uniformly distributed. The heterogeneous nucleation of the PAETE extrusion process tends to narrow the distribution of diameters of the PAETE bubbles. Subsequently, the PAETE bubbles

449





SEM micrograph of PMDA-ODA imidized from 50/50 blend in \sim 83.5% NMP. (a) Large phase-separated domains with diameters of 13-40 μ m are PAA-rich regions formed prior to soft bake. (b) Small dimples, \sim 700 nm in diameter, form during the hard-bake cycle. Dimples are shown on a phase-separated domain and on the surrounding surface.

imidize to PI(2) bubbles. Figure 8(b) shows the uniform size, ~700 nm, of such PI(2) bubbles on PI(1) mounds.

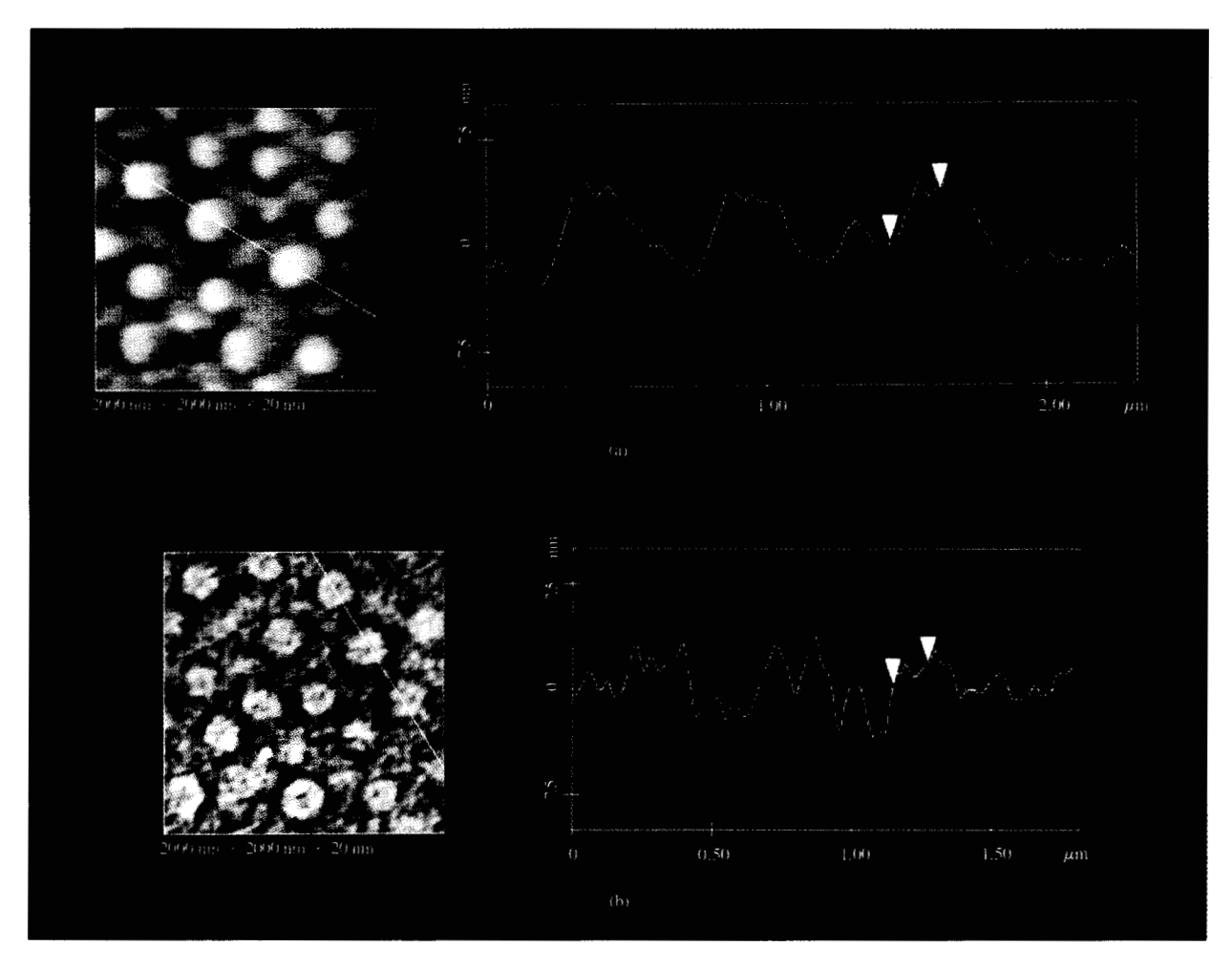
To understand the finer features on the region surrounding the mounds, the PATRP continuous region around the large mounds is considered. On drying, PATRP phases separate, as in Figure 4. On further hard bake, the morphology converts to the topography shown in Figure 6, with a continuous PI(2) domain and elevated discrete PI(1) bubbles. Figure 8(b) shows that the PI(1) bubbles on the continuous region around the mounds have a fairly uniform size distribution.

Heterogeneous ordering

The heterogeneous ordering process that disrupts the continuous ordered skin on the PI surface is considered next. The reason for heterogeneous ordering, based on AFM studies, and its effect on the structure of the skin are presented.

The cascaded imidization of PAA and PAETE leads to differences in the extent of order in PI(1) and PI(2). The

PAA → PI(1) in the PAA-rich phase occurs in a manner similar to conventional PI imidization. No significant plasticization due to PAETE is expected because T_a of PAETE is between 150 and 180°C; this indicates that the PAETE chain is nominally frozen during PAA imidization. However, when PAETE \rightarrow PI(2), significant ordering due to heterogeneous nucleation at the PAETE/PI(1) interface occurs and, as a consequence, PI(2) should be more ordered than PI(1). As mentioned earlier, a skin forms at the air/PI interface. Because of the cascaded imidization process, first the skin at the PI(1)/air interface forms, and this stage is followed by skin formation at the PI(2)/air interface. Since the PI(1) skin is already frozen (owing to high T_{σ} and low imidization temperature) when the PI(2) skin forms, the two skins are not connected. Such a heterogeneous ordering process breaks up the skin and improves adhesion by preventing delamination. Thus, observation of such a heterogeneous ordering process indicates a feature favorable for good adhesion.

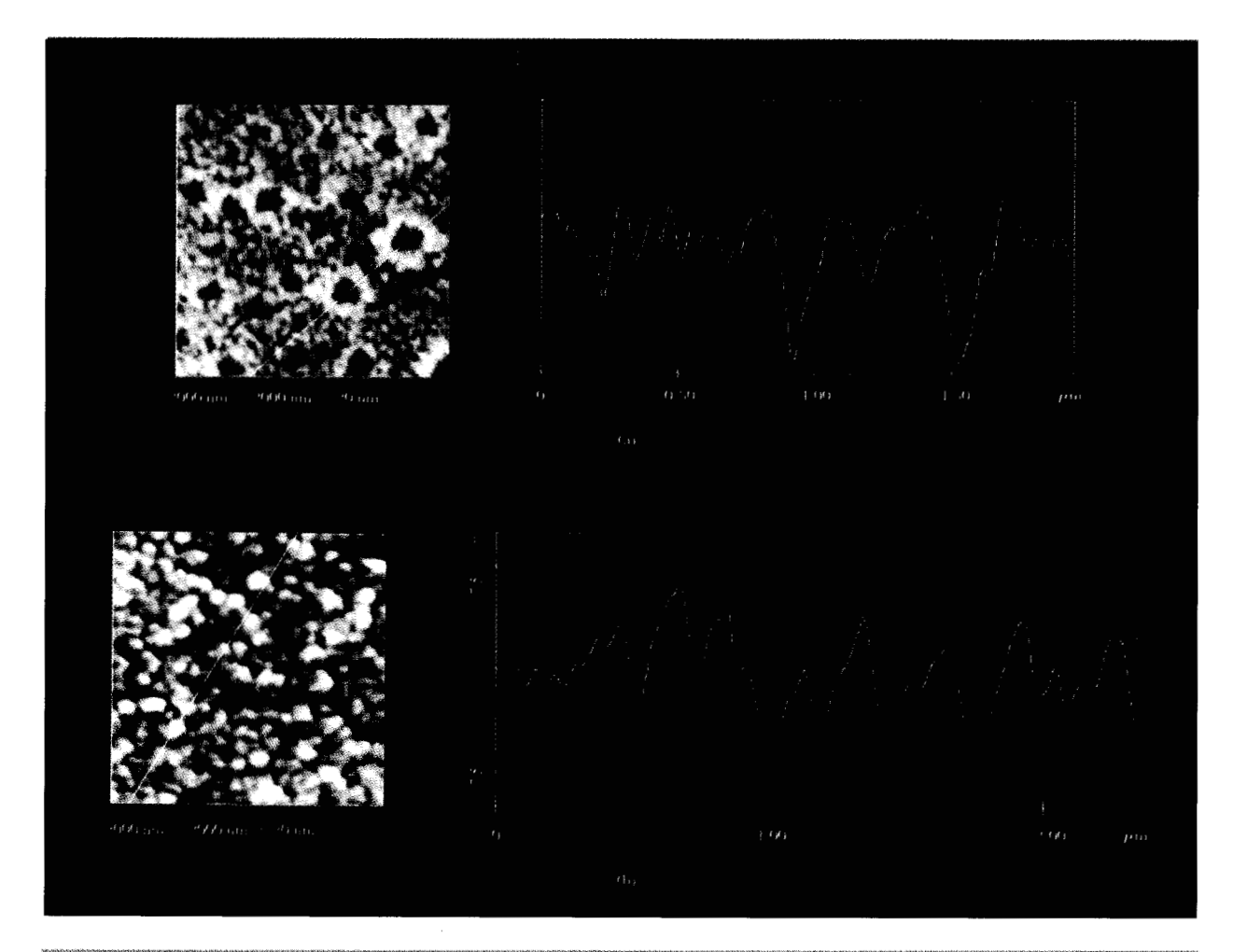


Secretary of the second

Typical locus of cross section and cross section of 20/80 blend, (a) before and (b) after etching. The sample before etching is hard-baked to 400°C in a forming gas atmosphere. The average height of the mounds decreases by \sim 45% due to 1 M KOH etching for 5 min and 1 M acetic acid ion exchange for 1 min, followed by NMP rinse and a soft-bake cycle at 70°C for 60 min. The vertical (and horizontal) distances between the red, green, and white markers in (a) are 3.732 nm (164 nm), 3.840 nm (164 nm), and 3.524 nm (180 nm), respectively. The vertical (and horizontal) distances between the red, green, and white markers in (b) are 2.221 nm (109 nm), 2.098 nm (172 nm), and 1.596 nm (125 nm), respectively. The nominal diameter of the features is given by twice the horizontal distance, and the vertical distance is the typical height of the mounds.

To measure heterogeneous ordering we observe the effect of etching on surface topography. Figure 9 shows the topography of a cured 20/80 blend before and after etching. The etching is performed with a 1 M KOH solution. The base attacks the imide linkage, forming a potassium salt of polyamic acid. The K^+ is then ion-exchanged with H^+ to form polyamic acid on the surface. The etched polymer is dissolved in solvent NMP. The typical cross-sectional view in Figure 9 indicates that the relative difference in elevation between PI(1) mounds and PI(2) land decreases by $\sim 30\%$ due to etching. Thus, the rate of etching of PI(1) is faster than that of PI(2). Since the rate of etching is

inversely proportional to the extent of order, PI(2) is more ordered than PI(1). The same conclusion is drawn from etching a film made from a cured 80/20 blend. The AFM scans in Figure 10 show that the dimples are barely visible after the etching process compared to the initial topography. The cross-sectional view of the topography before and after etching indicates a 45% decrease in depth, implying that the PI(1) land made from a PAA-rich phase etches at a faster rate than the PI(2) base of the dimples made from a PAETE-rich phase. Thus, the etching studies on films made from both PAA-rich and PAETE-rich blends are consistent and imply that PI(2) is more ordered than PI(1).



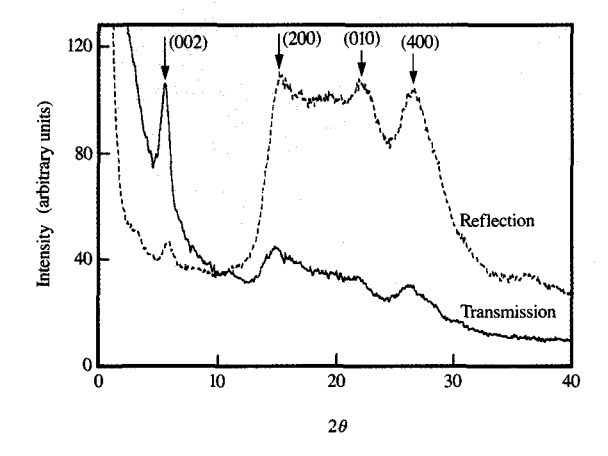
Floure 10

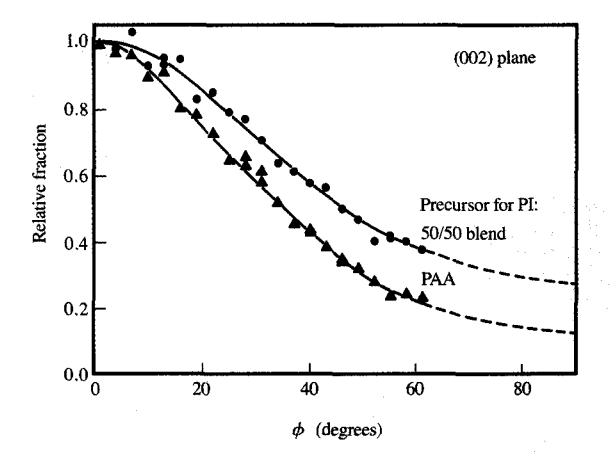
Typical locus of cross section and cross section of 80/20 blend, (a) before and (b) after etching. The sample before etching is hard-baked to 400° C in a forming gas atmosphere. The average height of the dimples decreases by $\sim 30\%$ due to 1 M KOH etching for 5 min and 1 M acetic acid ion exchange for 1 min, followed by NMP rinse and a soft-bake cycle at 70° C for 60 min. The vertical (and horizontal) distances between the red and green markers in (a) are 11.036 nm (106 nm) and 11.714 nm (121 nm), respectively. The vertical (and horizontal) distances between the red and green markers in (b) are 3.499 nm (125 nm) and 5.399 nm (98 nm), respectively. The nominal diameter of the features is given by twice the horizontal distance, and the vertical distance is the typical depth of the dimples.

• Chain orientation

The last structural feature we consider is the chain orientation in a cured PMDA-ODA film made from a blend. As mentioned earlier, the imidization of PAA and PAETE is a cascade process. As PAETE imidizes following PAA imidization, it has not only the polymer/air and polymer/substrate interface along which to orient, but also the PI(1)/PAETE interface. Since the latter interface is randomly oriented, the *c*-axis of PI(2) chains will be isotropic. Figure 1 and Figure 11 show the WAXS patterns of a fully imidized PI film made from PAA and a 50/50 blend, respectively. Although the film made from PAA is thicker, the peaks in the WAXS pattern of PI from a precursor blend are sharper. This is evident from a

comparison of the (010), (400), (200) peaks (in reflection mode) and the amorphous halo in the 15–20° 2θ range. For example, the (010) peak in Figure 11 is quite distinct in the reflection mode, while it is broad and overlapped by an amorphous halo in Figure 1. The (010), (400), and (200) peaks in Figure 1 are significantly weaker than those in Figure 11. This indicates that interchain packing in PMDA–ODA made from the precursor blend is better than the film from pure PAA. This is consistent with the etching experiments discussed in the preceding subsection. PI(2) showing more order than PI(1) leads to a higher overall order for samples made from a blend rather than from either single precursor (PAA or PAETE). The (002) peak is equally prominent in the two samples, indicating that the





WAXS spectra of a PMDA-ODA film imidized from 50/50 blend. The sample was soft-baked at 70°C for 30 min, followed by a 10°C/min ramp to 410°C. The hard bake at 410°C in a forming gas atmosphere was carried out for 60 min. The film was 109 μ m thick. The diffractograms are corrected for absorption, and the spectrum in transmission is multiplied by 2.

order along the chain direction for the two samples is nominally the same.

A comparison of the relative heights of the (002) peak in reflection and transmission modes indicates that the film in Figure 1 appears more oriented than the film in Figure 11. To make a more quantitative comparison of the orientation distribution of the two films, the complete pole-figure [40] for (002) reflection is considered. Since the chain orientation texture is planar, the orientation distribution with respect to the Z-axis is sufficient. Figure 12 compares the chain-axis orientation distribution of the two films in Figures 1 and 11. The population density is normalized with respect to $\phi = 0^{\circ}$, corresponding to in-plane chains. The change in (002) intensity was measured by scanning across the peak to ensure proper background subtraction. The change in path length due to ϕ is accounted for by experimentally measuring the mass-thickness absorption [40]. Although chains are oriented in both films, the distribution function for the PI from the blend is significantly broader than for the film from pure PAA. Quantitatively, the average chain orientation distribution, referred to as Herman's orientation function [40], has decreased by ~23% in the film made from the blend compared to one precursor. Thus, the film from the blend is less planar-oriented than the film from one precursor. Furthermore, the relative fraction of ordered chains in the off-plane directions increases significantly. For example, by extrapolating the curve to $\phi = 90^{\circ}$, the fraction of

Emilia 18

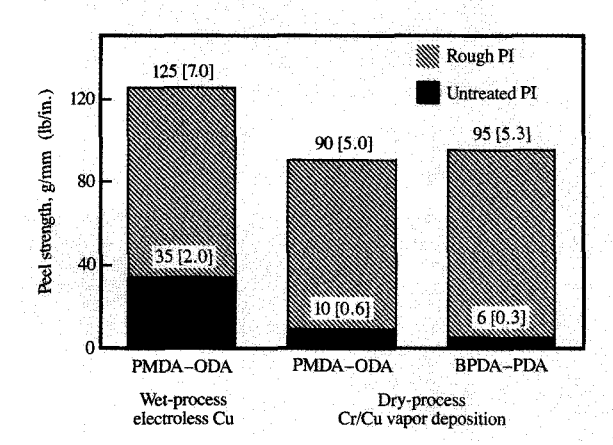
Normalized population distribution of the chain axes in PMDA-ODA film as a function of ϕ is obtained from the (002) reflection (ϕ is the angle between the chain axis and the X-Y plane). The orientation from 0° to 63° is obtained in transmission mode. The samples are identical to those of Figures 1 and 11. Herman's orientation functions obtained from the full-width-at-half-height for PAA and the 50/50 blend are 0.62 and 0.48, respectively. This 23% decrease indicates that the chains are more isotropic in the film from the 50/50 blend than in the one made from pure PAA.

chains increases from \sim 0.1 to \sim 0.2 in PI films made from blends compared to pure PAA (or PAETE). This increase is a more significant gain in the film structure than the decrease in orientation function, because the chains normal to the film plane contribute more to adhesion by interdigitating various layers to improve the fracture toughness and mechanical strength in the direction normal to the film.

The combined effect of a nanoscale roughened topography, heterogeneously ordered surface, and nonplanar chain orientation increases the toughness of the interface in three ways: First, the nanoscale roughening increases both the length and curvature of the locus of failure, e.g., at a Cu/PI interface, thus increasing the total work of adhesion. Second, making the ordered skin discontinuous increases the energy needed for crack propagation in the near-surface region. Third, decreasing the planar chain orientation distribution, and increasing the chain fraction normal to the surface plane, prevents delamination of the film by crack propagation between the film planes.

4. Electroless copper deposition process

Next we compare structurally modified and conventionally cured PMDA-ODA films with regard to adhesion of Cu. The metal is deposited by both (wet) electroless and (dry)



Peel strength of Cu deposited on PMDA-ODA and BPDA-PDA. The relative adhesion enhancement for PMDA-ODA (with respect to conventionally cured PI) is approximately threefold and ninefold for electroless and vapor deposition processes, respectively. An approximate ninefold enhancement in peel strength for BPDA-PDA is observed. No special surface preparation was performed for the vapor deposition process. The conventionally cured PI made from pure PAA or pure PAETE precursors was processed with the blend samples to ensure identical curing cycles.

vapor deposition processes. An electroless Cu deposition on a polymer is accomplished by seeding the polymer surface with Pd⁰ [41]. A cured PI film is treated with NaOH to form a Na salt with the PI [42]. The surfacemodified film is immersed in a palladium acetate solution which exchanges the Na⁺ with Pd⁺² ions [42]. The Pd⁺² is then reduced at the surface to elemental Pd in a NaBH, solution. Copper is deposited on the palladium-seeded PI surface using formaldehyde as a reducing agent and tartrate as a chelating agent to prevent precipitation of copper hydroxide [43]. An ~ 1 - μ m-thick film of Cu is deposited electrolessly. The thin Cu film, referred to as the strike layer, is annealed to 400°C. An \sim 10- μ m-thick electrolytic Cu film is deposited on the strike layer to perform a peel test. The adhesion measurement is performed at 1.25 mm/min, with a 3-mm-wide strip. Since the peel strength is sensitive to the film thickness, the plating times in both the electroless and electrolytic baths are kept constant. The Cu/PI adhesion measured by the peel test indicates a remarkable improvement in adhesion, as shown in Figure 13. Cu/PI adhesion for a 50/50 blend is 125 g/mm, in comparison to 35 g/mm for the pure PI made from PAA or PAETE. In one experiment, a peel strength of 140 g/mm for the 50/50 blend was measured. The high adhesion strength is attributed to the modified surface morphology and topography.

To further demonstrate the role of morphology, 20 nm of Cr followed by 1 μ m of Cu was vapor-deposited on a PI film. The film was subsequently electroplated with an additional 9 μ m of Cu. A similar adhesion enhancement is observed on the dry-deposited film, indicating that the increase was not due to the wet-processing steps. We note that peel strengths of 90 g/mm are obtained for dry process, without any special cleaning and surface modification steps that are usually employed in conventionally cured PI to improve adhesion (see Figure 13). Vapor deposition of Cu on BPDA-PDA films made from a 50/50 blend of its acid and ester precursors also resulted in adhesion improvement (Figure 13).

Since the adhesion strength required for a reliable Cu/PI interface is ~60 g/mm, the present method may prove to be a very important and useful technique for eliminating the application of Cr or other reactive metals to promote adhesion. It may make inexpensive wet deposition a viable technology compared to dry processing requiring high-vacuum systems. It is apparent that the scheme to tailor the morphology and topography of a PI may apply to all polyimides and other polymers that are processed in their precursor forms.

5. Conclusion

Adhesion enhancement by surface modification is well known. In this study, we show the relevance of tailoring surface morphology (i.e., chain orientation texture, skin formation, topography) to adhesion. We show that PI surfaces are not amenable to good adhesion because of the morphology of a conventionally cured film. The major morphological features detrimental to the interfacial toughness leading to poor adhesion are 1) spontaneous chain orientation parallel to the film plane; 2) the formation of an ordered PI surface; and 3) smooth surface topography. A new method of producing PI films is proposed and studied that replaces the one-precursor solution with a blend of two precursors, followed by an identical curing cycle. By regulating the blend composition and soft-bake conditions, a tougher metal/PI interface is obtained, as is evident from the enhanced Cu/PI adhesion. The method alters the PI morphology in three ways: first, the chain orientation is more isotropic; second, a discontinuous skin is produced; and third, a topographically rough surface is produced. These structural features are induced spontaneously during the imidization process, and the chemical composition of the PI (bulk and surface) is unchanged. For Cu deposited onto PMDA-ODA, a threefold and ninefold enhancement in adhesion relative to conventionally cured PI film is obtained for electroless and vapor-deposited Cu film, respectively.

References

- Microelectronics Packaging Handbook, R. R. Tummala and E. J. Rymaszewski, Eds., Van Nostrand Reinhold, New York, 1989.
- P. M. Cotts and W. Volksen, *Polymer News* 15, 106 (1990).
- F. W. Harris, in *Polyimides*, D. Wilson, H. D. Stenzenberger, and P. M. Hergenrother, Eds., Blackie & Sons, Glasgow, UK, 1990, p. 1.
- K. K. Chakravorty, J. M. Čech, C. P. Chien, L. S. Lathrop, M. H. Tanielian, and P. L. Young, J. Electrochem. Soc. 137, 961–966 (1990).
- R. Rubner, H. Ahne, E. Kuhn, and G. Kolodziej, *Photo. Sci. & Eng.* 23, 303 (1979).
- D. Wilson, in *Polyimides*, D. Wilson, H. D. Stenzenberger, and P. M. Hergenrother, Eds., Blackie & Sons, Glasgow, UK, 1990, p. 187.
- 7. P. Hergenrother, ibid., p. 158.
- F. Faupel, C. H. Chang, S. T. Chen, and P. S. Ho, J. Appl. Phys. 65, 1911 (1989).
- N. J. Chou, D. W. Dong, J. Kim, and A. C. Liu, J. Electrochem. Soc. 131, 2335 (1984).
- B. K. Furman, S. Purushothaman, E. Castellani,
 S. Renek, and D. Neugroshl, in *Metallization of Polymers*,
 ACS Symposium Series, Vol. 440, E. Sacher, J. J.
 Pireaux, and S. P. Kowalczyk, Eds., American Chemical Society, Washington, DC, 1990, p. 297.
- K. Bright, B. W. Malpass, and D. E. Packham, *Nature* 223, 1360 (1969).
- 12. I. A. Abu-Isa, Polymer-Plast. Technol. Eng. 2, 29 (1973).
- D. R. Fitchmun, S. Newman, and R. Wiggle, J. Appl. Polymer Sci. 14, 2411, 2457 (1970).
- E. J. O'Sullivan, T. R. O'Toole, J. M. Roldan, L. T. Romankiw, C. J. Sambucetti, and R. Saraf, U.S. Patent 5,310,580, October 5, 1994.
- L. G. Kazaryan, D. Ya. Tsvankin, B. M. Ginsburg, Sh. Tuichiev, L. N. Korzhavin, and S. Ya. Frenkel, Vysokomol. Soedin. Ser. A 14, 1199 (1972); Polymer Sci. USSR (English translation) 14, 1344 (1972).
- A. V. Sidorovich, Yu. G. Baklagin, A. V. Kenarov, Yu. S. Nadezhin, N. A. Adrova, and F. S. Florinsky, J. Polymer Sci. Polymer Symp. 58, 359 (1977).
- G. Conte, L. Iliaro, N. V. Patel, and E. Giglio, J. Polymer Sci., Polymer Phys. Ed. 14, 1553 (1976).
- T. W. Poon, R. F. Saraf, and B. D. Silverman, Macromolecules 26, 3369 (1993).
- T. P. Russell, H. Gugger, and J. D. Swalen, J. Polymer Sci., Polymer Phys. Ed. 21, 1745 (1983).
- 20. R. F. Saraf, Polymer 35, 1359 (1994).
- J. Y. Guan, R. F. Saraf, and R. S. Porter, J. Appl. Polymer Sci. 33, 1517 (1987).
- L. Holliday, in Structure and Properties of Oriented Polymers, I. M. Ward, Ed., John Wiley & Sons, Inc., New York, 1975, p. 242.
- H. Jacque and I. G. Farben, U.S. Patent 2,185,789, 1936;
 O. B. Rasmussen, Text. Inst. Industr. 2, 258 (1964).
- 24. R. F. Saraf and R. S. Porter, J. Rheol. 31, 59 (1987).
- H. Dosch, Critical Phenomena at Surfaces and Interfaces, Springer-Verlag, Heidelberg, Germany, 1992; R. F. Saraf, in Practical Guide to Characterization of Polymer Surfaces and Interfaces, H. M. Tong, R. F. Saraf, and S. P. Kowalczyk, Eds., Butterworth-Heinemann Publishers, Stoneham, MA, 1994.
- B. J. Factor, T. P. Russell, and M. F. Toney, *Phys. Rev. Lett.* 66, 1181 (1991).
- R. F. Saraf, J. M. Lefebvre, R. S. Porter, and G. D. Wignall, MRS Symp. Proc. 79, 263 (1987).
- K. L. Mittal, J. Vac. Sci. Technol. 13, 19 (1976); C. J. Cahn, J. Adhesion 15, 217 (1983); L. P. Buchwalter, J. Adhesion Sci. Technol. 7, 941 (1993).

- R. J. Young, R. J. Day, and M. Zakipkskhani, *Mater. Res. Soc. Symp. Proc.* 134, 351 (1989); D. C. Martin and E. L. Thomas, *ibid.*, 134, 465 (1989); D. C. Sawyer and M. Jaffe, *J. Mater. Sci.* 21, 1897 (1986).
- S. K. Sinha, E. B. Sirota, S. Garoff, and H. B. Stanley, *Phys. Rev. B* 38, 2297 (1988).
- R. F. Saraf, in Practical Guide to Characterization of Polymer Surfaces and Interfaces, H. M. Tong, R. F. Saraf, and S. P. Kowalczyk, Eds., Butterworth-Heinemann Publishers, Stoneham, MA, 1994, p. 121.
- 32. D. J. Arrowsmith, Trans. Inst. Met. Finish. 48, 88 (1970).
- B. W. Malpass, D. E. Packham, and K. Bright, J. Appl. Polymer Sci. 18, 3249 (1974).
- P. Blais, D. J. Carlsson, G. W. Csullog, and D. M. Wiles, J. Colloid Interface Sci. 47, 636 (1974).
- B. J. Briscoe and S. S. Panesar, J. Phys. D: Appl. Phys. 25, A20 (1992).
- M. J. Brenker and C. Feger, J. Polymer Sci. Polymer Chem. Ed. 25, 2005–2020 (1987).
- N. C. Stoffel, E. J. Kramer, W. Volkeson, and T. P. Russell, *Polymer* 34, 4524 (1993).
- 38. R. F. Saraf, Macromolecules 26, 3623 (1993).
- J. A. Kreuz, A. L. Endrey, F. B. Gay, and C. E. Sroog, J. Polymer Sci. 4, 2607 (1966).
- L. E. Alexander, X-Ray Diffraction Methods in Polymer Science, Krieger Publishing Co., Huntington, NY, 1979.
- 41. J. Horkans, J. Kim, C. McGrath, and L. T. Romankiw, J. Electrochem. Soc. 134, 300 (1987).
- 42. M. M. Plechaty and R. R. Thomas, *J. Electrochem. Soc.* 139, 810–821 (1992).
- F. Pearlstein, in Modern Electroplating, Third Ed., F. A. Lowenheim, Ed., John Wiley & Sons, Inc., New York, 1974, pp. 710-747.

Received December 1, 1993; accepted for publication June 9, 1994

Ravi F. Saraf IBM Research Division, Thomas J. Watson Research Center, P.O. Box 218, Yorktown Heights, New York 10598 (SARAF at YKTVMV, saraf@watson.ibm.com). Dr. Saraf is a Research Staff Member in the Silicon Science and Technology Department at the IBM Thomas J. Watson Research Center. He received his B.Tech. from the Indian Institute of Technology, Kanpur, in 1979, and his Ph.D. from the University of Massachusetts at Amherst in 1986. He subsequently joined the Research Center, where he has worked on physical structure and properties of polymers. Dr. Saraf has received two IBM Invention Achievement Awards, in 1991 and 1992, respectively, and has co-edited a book on the characterization of polymer surfaces. He is a member of the American Physical Society.

Judith M. Roldan IBM Research Division, Thomas J. Watson Research Center, P.O. Box 218, Yorktown Heights, New York 10598 (TWEEDIE at YKTVMT). Mrs. Roldan is a Senior Associate Engineer in the Advanced Manufacturing Technologies Department at the Thomas J. Watson Research Center, working on interconnection materials. She received a B.A. from Manhattanville College in 1981 and an M.S. from Long Island University in 1985, both in chemistry. Mrs. Roldan is a member of the American Chemical Society.

Theresa Derderian Bio Med Sciences, 101 Technology Drive, Bethlehem, Pennsylvania 18015. As a summer intern, Ms. Derderian worked in the Manufacturing Research Department at the IBM Thomas J. Watson Research Center; she received her B.S. degree in materials science and engineering from M.I.T. in 1992. After receiving her M.S. degree in materials science and engineering from the University of Pennsylvania in 1993, she began working for Bio Med Sciences as an Applications Development Manager. Ms. Derderian is a member of the Society for Biomaterials.